Wake Vortex Effects Between Urban Air Mobility Aircraft

Joshua Baculi*

HX5, LLC., Moffett Field, CA 94035

Nhan Nguyen†

NASA Ames Research Center, Moffett Field, CA 94035

Wendy A. Okolo‡

NASA Ames Research Center, Moffett Field, CA 94035

Juntao Xiong§

KBR Wyle, Inc., Moffett Field, CA 94035

This study models the wake-induced downwash of an Urban Air Mobility (UAM) aircraft and the wake's effects on a trailing aircraft's dynamic stability when intersecting the wake trail. The Proctor wake vortex model is used to compute the wake-induced downwash over a 0.8 $\times$ 0.8 nautical mile flight area. The model is complemented by core radius growth, Proctor single phase wake decay, wake propagation, and Lamb wake aging. The wake data is then stored and loaded to the trailing aircraft as an atmospheric condition to affect the dynamics. Preliminary simulations include modeling the downwash from multiple UAM aircraft over the flight area and determining the normalized wake reduction at the ICAO 5 nautical mile separation criteria for a LIGHT aircraft trailing a MEDIUM aircraft.

I. Introduction

The growth in urban population densities has motivated the need for revolutionary transportation solutions such as air taxis. The Urban Air Mobility (UAM) concept strives to develop infrastructure and technology to achieve such solutions. Looking at the existing airspace infrastructure as a reference, the densest operations center around airports where the separation criteria between aircraft is clearly defined by policy/regulation and supported by the physical infrastructure. However, this is not the case in the urban setting where high-rise buildings and narrow streets do not conform to such separation criteria. Therefore, forming the UAM airspace will not be a simple translation of existing infrastructure.

To overcome safety challenges such as the wake separation in the urban environment, the System-Wide Safety (SWS) project under NASA's Aeronautics Research Mission Directorate (ARMD) is researching solutions for novel small Unmanned Aircraft Systems (sUAS) and UAM operations.[1] One of the project's technical challenges is focused on mitigating safety-oriented operational hazards such as critical system failures, propulsion component degradation, and engine/power failure.[2] Through SWS, a hazard such as

*Systems Engineer, HX5, LLC., NASA Ames Research Center, Moffett Field, CA 94035, AIAA Member, joshua.e.baculi@nasa.gov.

†Senior Research Scientist and Technical Group Lead of Advanced Control and Evolvable Systems Group, Intelligent Systems Division, AIAA Associate Fellow, nhan.t.nguyen@nasa.gov.

‡Research Scientist, Intelligent Systems Division, wendy.a.okolo@nasa.gov.

§Aerospace Engineer, Intelligent Systems Division, juntao.xiong@nasa.gov.

wake-induced downwash in autonomous operations can be modeled for monitoring and predicting in real-time when the risk exceeds safety thresholds. In the event of unsafe conditions, the autonomous aircraft or human-in-the-loop is informed of the situation to make a mitigating decision.

To date, various aircraft wake models[3] have been tested in simulation[4] and experiment[5] to observe the effects on incoming aircraft. Where this study looks to differentiate from past studies is the inclusion of a physics-based aircraft model for evaluating the wake effects on a simulated small autonomous aircraft. By using high-fidelity models, we achieve greater flexibility in testing a variety of aircraft models as well as a more nuanced understanding on the effects of flight stability and dynamics and how they can determine model-specific separation criteria.

A. Contribution

This paper builds upon previous work[6,7] studying UAM aircraft-generated wake vortices. The previously developed wake models are simulated in Matlab to generate wake time histories over a flight area large enough for multiple UAM operations like the one shown in Figure 1. A 6 degree of freedom (6DOF) UAM aircraft is numerically simulated to fly through a leading UAM aircraft's wake trail to observe the effects on the incoming aircraft's dynamics. In summary, this study can be split into two parts:

- Wake vortex simulation over a fixed area.
  - Wake vortex model.
  - Separation assurance criteria.
  - Wake velocity datasets.
- UAM aircraft wake response.
  - Aircraft 6DOF equations of motion.
  - Stability and dynamics derivatives.
  - Wake effects on aircraft stability.

This abstract covers the first part focusing on the wake vortex simulation. The results of the UAM wake response will be added in the final manuscript.

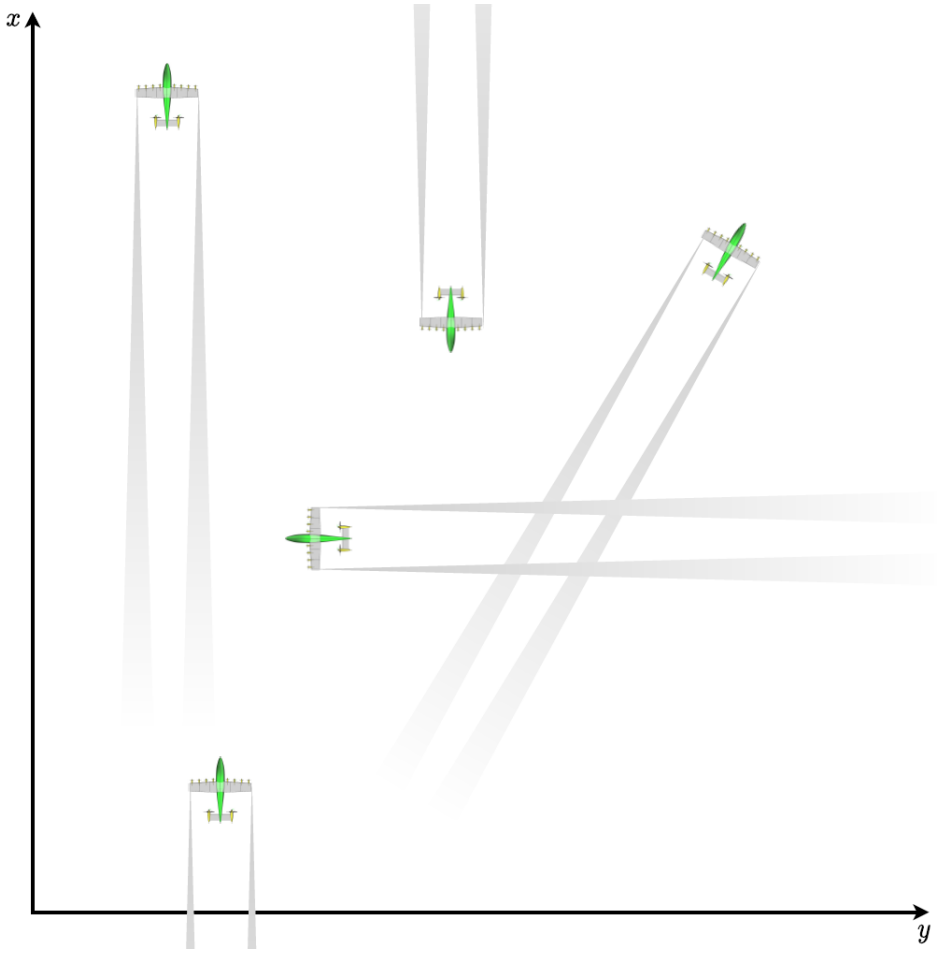

Figure 1: UAM operations in dense airspace where wake intersections may occur. Wake cores are shown in gray gradients trailing aircraft (not shown to scale).

II. Wake Vortex Model

Aircraft wake vortices are the result of complex aeroelastic interactions between the lifting surfaces and surrounding airstream. The high and low pressure distribution respectively below and above the lifting surface roll outwards until they meet at the tip where vortices are created. Figure 2 shows the wake vortex distribution trailing a fixed-wing aircraft and how the opposing rotational direction of the tip vortices compound to create a net downwash between the tips and upwashes outside.

A. Simplified Aircraft Model

To compute the wake-induced downwash, we focus our study to simple fixed-wing aircraft whose relevant parameters consist of the weight W, wing span b, lifting surface area S, and span efficiency factor ε. For the fixed-wing in this study, we focus on a rectangular wing as the sole lifting surface. Rotorcraft wake vortex models can be found in other literature[7]

B. Relative Positions

The dense UAM airspace shown in Figure 1 is isolated to a single UAM aircraft and an arbitrary point of interest c in Figure 3. The aircraft has a forward-right-down body frame $\{\mathbf{i}_b, \mathbf{j}_b, \mathbf{k}_b\}$ that is related to the North-East-Down inertia frame $\{\mathbf{i}, \mathbf{j}, \mathbf{k}\}$ by the coordinate transformation in Equation 1. The inverse of this

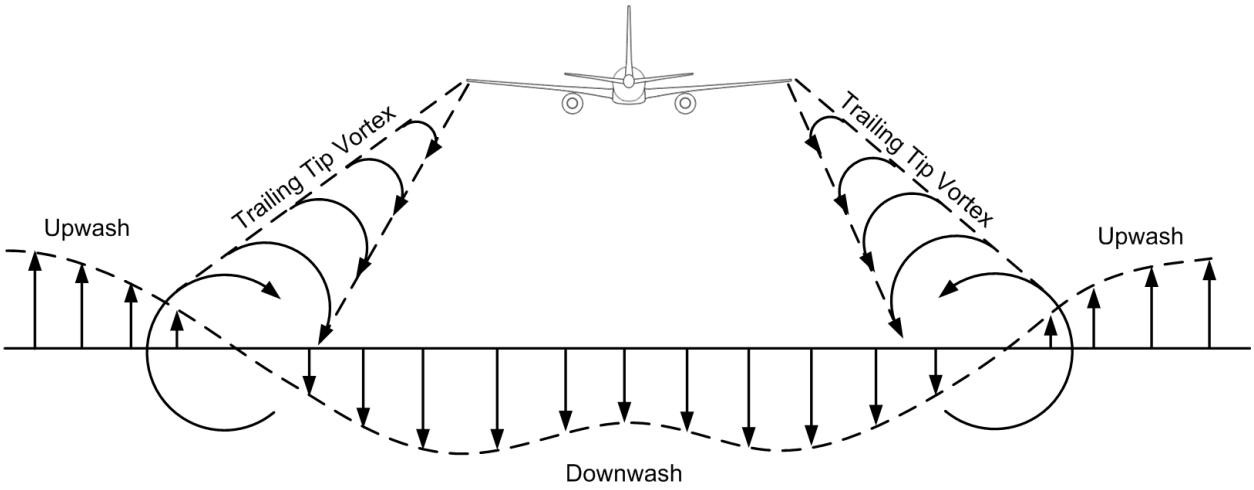

Figure 2: Aircraft downwash distribution.

transformation is shown in Equation 2. ϕ, θ, and ψ are the roll, pitch, and yaw angles, respectively.

$$\begin{bmatrix} \mathbf{i}_b \\ \mathbf{j}_b \\ \mathbf{k}_b \end{bmatrix} = \begin{bmatrix} \cos\theta\cos\psi & \cos\theta\sin\psi & -\sin\theta \\ -\cos\phi\sin\psi + \sin\phi\sin\theta\cos\psi & \cos\phi\cos\psi + \sin\phi\sin\theta\sin\psi & \sin\phi\cos\theta \\ \sin\phi\sin\psi + \cos\phi\sin\theta\cos\psi & -\sin\phi\cos\psi + \cos\phi\sin\theta\sin\psi & \cos\phi\cos\theta \end{bmatrix} \begin{bmatrix} \mathbf{i} \\ \mathbf{j} \\ \mathbf{k} \end{bmatrix} \tag{1}$$

$$\begin{bmatrix} \mathbf{i} \\ \mathbf{j} \\ \mathbf{k} \end{bmatrix} = \begin{bmatrix} \cos\theta\cos\psi & -\cos\phi\sin\psi + \sin\phi\sin\theta\cos\psi & \sin\phi\sin\psi + \cos\phi\sin\theta\cos\psi \\ \cos\theta\sin\psi & \cos\phi\cos\psi + \sin\phi\sin\theta\sin\psi & -\sin\phi\cos\psi + \cos\phi\sin\theta\sin\psi \\ -\sin\theta & \sin\phi\cos\theta & \cos\phi\cos\theta \end{bmatrix} \begin{bmatrix} \mathbf{i}_b \\ \mathbf{j}_b \\ \mathbf{k}_b \end{bmatrix} \tag{2}$$

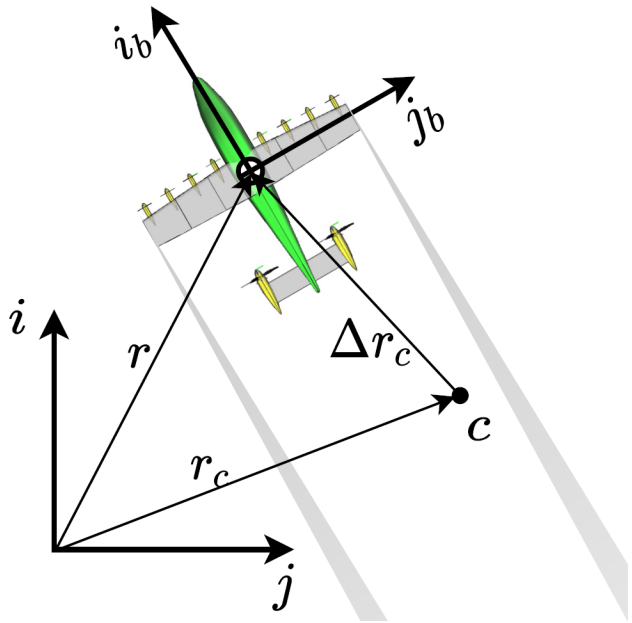

Figure 3: Aircraft position relative to arbitrary point within wake field viewed on horizontal plane.

The position of point c relative to the aircraft CG is denoted as Δr_c in Figure 3 and given by Equation

3.

$$\begin{aligned}\Delta\mathbf{r}_c &= \mathbf{r} - \mathbf{r}_c \\ &= (x - x_c)\mathbf{i} + (y - y_c)\mathbf{j} + (z - z_c)\mathbf{k} \\ &= \Delta x_c\mathbf{i} + \Delta y_c\mathbf{j} + \Delta z_c\mathbf{k} \end{aligned} \tag{3}$$

Using the coordinate transform in Equation 1, the components of Equation 3 can be rewritten in the aircraft body frame

$$\Delta x = \Delta x_c(\cos\theta\cos\psi) + \Delta y_c(\cos\theta\sin\psi) - \Delta z_c(\sin\theta) \tag{4}$$

$$\Delta y = \Delta x_c(-\cos\phi\sin\psi + \sin\phi\sin\theta\cos\psi) + \Delta y_c(\cos\phi\cos\psi + \sin\phi\sin\theta\sin\psi) + \Delta z_c(\sin\phi\cos\theta) \tag{5}$$

$$\Delta z = \Delta x_c(\sin\phi\sin\psi + \cos\phi\sin\theta\cos\psi) + \Delta y_c(-\sin\phi\cos\psi + \cos\phi\sin\theta\sin\psi) + \Delta z_c(\cos\phi\cos\theta) \tag{6}$$

These $\Delta\cdot$ values are later used in modeling the wake propagation as a function of the distance from the point c to the wing tips L, R.

Because the wake vortices originate at the wing tips, we calculate the position of c relative to the tips L, R. Assuming the wing tips are aligned with the aircraft CG, $x_{L,R/b}$ and $y_{L,R/b}$ are aligned with the origin of the body frame in the x- and z-directions. Equations 7 and 8 show the wing tip location in the body and inertia frames, respectively, with the operand $\mp$ corresponding to the left L and right R wing tips, respectively.

$$\mathbf{r}_t = \pm\frac{b}{2}\mathbf{j}_b \tag{7}$$

$$= \pm\frac{b}{2}(-\cos\phi\sin\psi + \sin\phi\sin\theta\cos\psi)\mathbf{i} \pm \frac{b}{2}(\cos\phi\cos\psi + \sin\phi\sin\theta\sin\psi)\mathbf{j} \pm \frac{b}{2}(\sin\phi\cos\theta)\mathbf{k} \tag{8}$$

The position of point c can thus be written relative to the tips in the body frame

$$\begin{aligned} x_{c/L,R} &= \Delta x \\ y_{c/L,R} &= \Delta y \mp \frac{b}{2} \\ z_{c/L,R} &= \Delta z \end{aligned} \tag{9}$$

where, again, the operand $\mp$ corresponds to the left and right wing tips, respectively.

C. Lamb-Oseen Wake Model

The tangential wake velocity shown in Figure 4 can be modeled using a simple potential flow two-dimensional vortex model

$$v_\theta = \frac{\Gamma_0}{2\pi r} \tag{10}$$

where Γ_0 is the initial vortex circulation strength given by

$$\Gamma_0 = \frac{2C_L V S}{\pi b} = \frac{4L}{\pi\rho V b} \tag{11}$$

and $q = \frac{1}{2}\rho V^2$ is the dynamic pressure. For the simplified fixed-model that generates the wake vortices, the lift coefficient C_L and lift L in Equation 11 are assumed to be

$$C_L = \frac{W}{qS} \tag{12}$$

$$L = C_L q S \tag{13}$$

In Figure 4, v_θ lies on the plane perpendicular to the aircraft's forward body-axis x_b. r is the radial distance from the wing tip on this perpendicular plane and is denoted by

$$r = \sqrt{(\Delta y \mp \frac{b}{2})^2 + \Delta z^2} \tag{14}$$

The core radius r_c is given by Equation 15 and is defined to be the distance from the wing tip to where the tangential velocity v_θ is at maximum. Experiments conducted on Boeing 727, 757, and 767 fixed-wings measured the core radii to be consistently around 1% of the wing span.[1] We choose a measured core radius of the Boeing 757 as our initial value $r_c(0) = 0.014b$.

$$r_c(t) = \sqrt{r_c^2(0) + r\alpha_L \nu t} \tag{15}$$

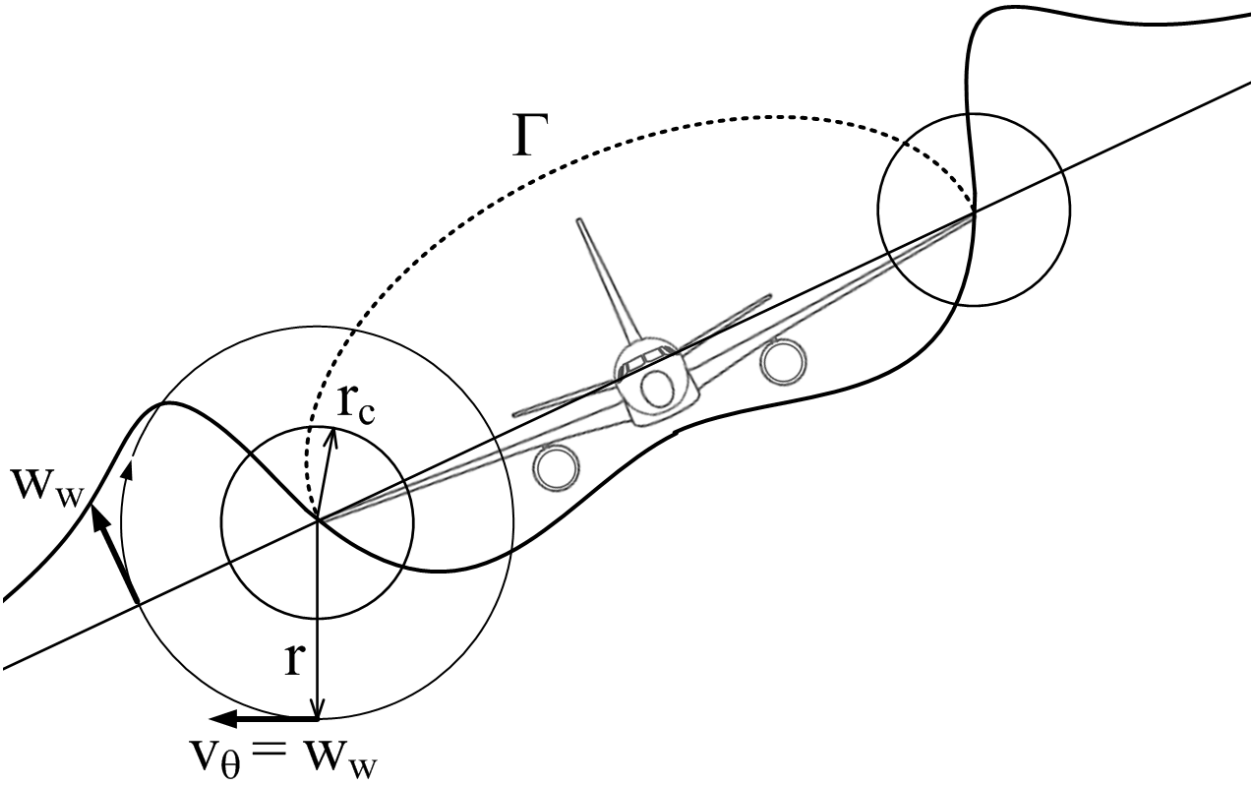

Figure 4: Aircraft wake vortices centered around the wing tips.

The Lamb-Oseen wake vortex model is an analytical solution to the Navier-Stokes equations[3] and is given by

$$v_\theta = \frac{\Gamma_0}{2\pi r}\left[1 - e^{-\alpha_L\left(\frac{r}{r_c}\right)^2}\right] \tag{16}$$

where $\alpha_L = 1.25643$. Equation 16 shows that the tangential velocity starts at zero at $r = 0$ and asymptotically converges to the simple potential flow model in Equation 10 as $r \to \infty$.

D. Proctor Wake Model

The Proctor wake model[8] outlined in Equation 17 is based on LIDAR measurements of fixed-wing flight and corrects for the effect of the wing span that is not considered in the Lamb-Oseen model by adding an amplitude correction term:

$$w_w = \begin{cases} \dfrac{\Gamma_0}{2\pi r}\left[1 - e^{-10\left(\frac{1.4r_c}{b}\right)^{0.75}}\right]\left[\dfrac{1 - e^{-\alpha_p\left(\frac{r}{r_c}\right)^2}}{1 - e^{-\alpha_p(1.4)^2}}\right] & r \le 1.4r_c \\ \dfrac{\Gamma_0}{2\pi r}\left[1 - e^{-10\left(\frac{|r|}{b}\right)^{0.75}}\right] & r > 1.4r_c \end{cases} \tag{17}$$

where $\alpha_p = 1.2527$.

To consider the transience of the wake model, Proctor et al. conducted large eddy simulations to come up with a three-phased wake vortex decay model.[9] Phase 1 consists of tip vortices that are longitudinally consistent while remaining separate and can be modeled using the Proctor model shown in Equation 17. Phase 2 occurs when the tip vortices begin linking and the wake rapidly decays. The linking vortices coalesce into a ring in Phase 3 and the decay slows back down.

We use the conservative approach from Nguyen et al.[7] that curve fits the first phase of the Proctor wake aging with the parameters from Table 1. Thus, the wake aging α can be written as a function of the eddy dissipation parameter ε^*:

$$\alpha = 0.3146\varepsilon^{*2} + 0.1108\varepsilon^* + 0.0453 \tag{18}$$

We assume $\varepsilon^* = 0.03$, resulting in $\alpha = 0.0489$.

Table 1: Wake age parameter α and corresponding eddy dissipation parameter ε^*.[7]

ε^*	α
0.03	0.04887
0.15	0.06896
0.5	0.17929

The wake decay is thus defined using a simple exponential model

$$\Gamma(t) = \Gamma_0 e^{-\alpha T} \tag{19}$$

where non-dimensional time T, initial vortex separation b_0, and initial vortex velocity V_0 are given as

$$T = \frac{tV_0}{b_0} \tag{20}$$

$$b_0 = \frac{\pi}{4} b \tag{21}$$

$$V_0 = \frac{\Gamma_0}{2\pi b_0} \tag{22}$$

Thus, the Proctor wake decay can be written as

$$\Gamma(t) = \Gamma_0 e^{-\alpha \frac{t\Gamma_0}{2\pi b_0^2}} \tag{23}$$

E. Boeing Propagation Model

We add a propagation parameter D to Equation 23 that is calculated using ground-based wake measurements of a Boeing 747 aircraft.[10] We apply a Web Digitizer on the "Circulation Time History for Flyby 44"[10] to formulate the wake propagation. The curve fit is linear between 0 to 33 wingspans downstream (Equation 24) and linear in a log-log scale (Equation 25) from 33 to 150 wingspans:

$$P_1 = a_1 x + b_1 \tag{24}$$

$$P_2 = x^{a_2} e^{b_2} \tag{25}$$

where $x = \Delta x/b$, $a_1 = 2.298 * 10^{-17}$, $b_1 = 1$, $a_2 = -1.002$, and $b_2 = 3.501$

Equations 24 and 25 are combined in a Heaviside function to fill out the propagation parameter D in Equation 26. We use $k = 12$ and $n = 33.2$.

$$D(\Delta x) = \frac{P_1}{1 + e^{k(x-n)}} + \frac{P_2}{1 + e^{-k(x-n)}} \tag{26}$$

The propagation circulation Γ_p can then be calculated using the initial circulation Γ_0 and propagation parameter D

$$\Gamma_p = \Gamma_0 D(\Delta x) \tag{27}$$

Γ_p is then substituted into Equation 23 to give

$$\begin{aligned}\Gamma(t,\Delta x) &= \Gamma_p e^{-\alpha\frac{t\Gamma_p}{2\pi b_0^2}} \\ &= D(\Delta x)\Gamma_0 e^{-\alpha\frac{tD(\Delta x)\Gamma_0}{2\pi b_0^2}}\end{aligned} \tag{28}$$

F. Complete Wake Model

The viscous dissipation of a wake vortex can be observed using the following Lamb model

$$v_\theta(t) = v_\theta(0)(1 - e^{-\frac{r^2}{4\nu t}}) \tag{29}$$

The Lamb aging model in Equation 29 and the Proctor wake decay model with propagation in Equation 28 are applied to Equation 17 to consider the spatial-temporal distribution of the wake:

$$w_w = \begin{cases} \dfrac{\Gamma(t,\Delta x)}{2\pi r}\left[1 - e^{-10\left(\frac{1.4r_c}{b}\right)^{0.75}}\right]\left[\dfrac{1 - e^{-\alpha_p\left(\frac{r}{r_c}\right)^2}}{1 - e^{-\alpha_p(1.4)^2}}\right]\left(1 - e^{-\dfrac{r^2}{4\nu t}}\right) & r \le 1.4r_c \\ \dfrac{\Gamma(t,\Delta x)}{2\pi r}\left[1 - e^{-10\left(\frac{|r|}{b}\right)^{0.75}}\right]\left(1 - e^{-\dfrac{r^2}{4\nu t}}\right) & r > 1.4r_c \end{cases} \tag{30}$$

The wake-induced downwash due to the wing tips is written in the inertia frame using Equations 30 and 8

$$U_w = \frac{w_w}{r}\left[-\Delta z(-\cos\phi\sin\psi + \sin\phi\sin\theta\cos\psi) + (\Delta y \mp \frac{b}{2})(\sin\phi\sin\psi + \cos\phi\sin\theta\cos\psi)\right] \tag{31}$$

$$V_w = \frac{w_w}{r}\left[-\Delta z(\cos\phi\cos\psi + \sin\phi\sin\theta\sin\psi) + (\Delta y \mp \frac{b}{2})(-\sin\phi\cos\psi + \cos\phi\sin\theta\sin\psi)\right] \tag{32}$$

$$W_w = \frac{w_w}{r}\left[-\Delta z\sin\phi\cos\theta + (\Delta y - \mp\frac{b}{2})\cos\phi\cos\theta)\right] \tag{33}$$

where the operand $\mp$ continues to correspond to the left and right wing tips, respectively.

Finally, the wakes induced by the left (L) and right (R) wing tips are summed to get the total downwash distribution in the inertia frame:

$$\begin{aligned} U_{w,tot} &= U_{w,L} + U_{w,R} \\ V_{w,tot} &= V_{w,L} + V_{w,R} \\ W_{w,tot} &= W_{w,L} + W_{w,R} \end{aligned} \tag{34}$$

III. Aircraft Model

While Section II used simplified fixed-wing model to simulate the wake-induced downwash, we need a 6 degree of freedom (6DOF) aircraft model to accurately simulate the dynamic response when flying through a wake trail. The wake is input to the 6DOF model using the stability frame shown below

$$\begin{bmatrix} \mathbf{i}_b \\ \mathbf{j}_b \\ \mathbf{k}_b \end{bmatrix} = \begin{bmatrix} \cos\theta\cos\psi & \cos\theta\sin\psi & -\sin\theta \\ -\cos\phi\sin\psi + \sin\phi\sin\theta\cos\psi & \cos\phi\cos\psi + \sin\phi\sin\theta\sin\psi & \sin\phi\cos\theta \\ \sin\phi\sin\psi + \cos\phi\sin\theta\cos\psi & -\sin\phi\cos\psi + \cos\phi\sin\theta\sin\psi & \cos\phi\cos\theta \end{bmatrix} \begin{bmatrix} \mathbf{i} \\ \mathbf{j} \\ \mathbf{k} \end{bmatrix} \tag{35}$$

Flight dynamics equations for an aircraft in a windfield:

$$\dot{u} + qw - rv = \frac{X+T}{m} - g\sin\theta - \dot{u}_b \tag{36}$$

$$\dot{v} + ru - pw = \frac{Y}{m} + g\cos\theta\sin\phi - \dot{v}_b \tag{37}$$

$$\dot{w} + pv - qu = \frac{Z}{m} + g\cos\theta\cos\phi - \dot{w}_b \tag{38}$$

$$I_{xx}\dot{p} - I_{xz}\dot{r} - I_{xz}pq + (I_{zz} - I_{yy})qr = l \tag{39}$$

$$I_{yy}\dot{q} + (I + xx - I_{zz})pr + I_{xz}(p^2 - r^2) = m + Tz_e \tag{40}$$

$$-I_{xz}\dot{p} + I_{zz}\dot{r} + I_{xz}qr + (I_{yy} - I_{xx})pq = n \tag{41}$$

m is the aircraft mass, I_{xx}, I_{yy}, I_{zz}, I_{xz}, and I_{yz} are the aircraft inertias, and z_e is the offset between the thrust vector whose magnitude is T and the aircraft center of mass. X, Y, and Z are the axial, side, and normal forces and l, m, and n are the rolling, pitching, and yawing moments applied to the aircraft. These values will be further developed in the final manuscript that covers the wake effects on aircraft stability and dynamics.

IV. Simulation

A. Separation Criteria

Table 2 shows the separation criteria required by the International Civil Aviation Organization (ICAO) between fixed-wing aircraft based on sizes shown in Table 3. The Boeing 747 data used to formulate the propagation model in Section II.E is listed as 493835 lbs,[10] putting it in the HEAVY category for fixed-wings.

Table 2: Distance-based wake turbulence separation minima for varying aircraft sizes.[11]

Preceding Aircraft	Succeeding Aircraft	Separation Minima
HEAVY	HEAVY	7.4 km (4.0 NM)
	MEDIUM	9.3 km (5.0 NM)
	LIGHT	11.1 km (6.0 NM)
MEDIUM	LIGHT	9.3 km (5.0 NM)

Table 3: FAA aircraft classes based on takeoff weight.

Class	Weight (lbs)
SUPER	Airbus A388 & Antonov A225
HEAVY	≥300,000
LARGE	41,000< & <300,000
SMALL	≤41,000

To gain an understanding of the downwash an incoming aircraft would experience when trailing the wake of another aircraft, we first simulated the wake produced by a Boeing 747-100 fixed-wing. Table 4 shows that at 735000 lbs, the B747-100 falls under the HEAVY category. Figure 5 shows the normalized downwash versus the downstream distance, where the normalized downwash is the downwash at that downstream distance divided by the initial downwash. At the 4, 5, and 6 nautical mile separation distances given in Table 2, the normalized downwashes were 0.257, 0.205 and 0.170, respectively.

The 5000 lb UAM aircraft described in Table 4 falls well below the LIGHT weight class defined in Table 3 by a factor of 8. There is also no separation criteria defined for two LIGHT aircraft, with the closest scenario

Table 4: FAA aircraft classes based on takeoff weight.

Aircraft	Boeing 747-100	UAM
Type	Fixed-Wing	Fixed-Wing
Weight W (lbs)	735,000	5,000
Class	HEAVY	LIGHT
Lifting Surface S (ft^2)	5,500	180
Wingspan b (ft)	195	30

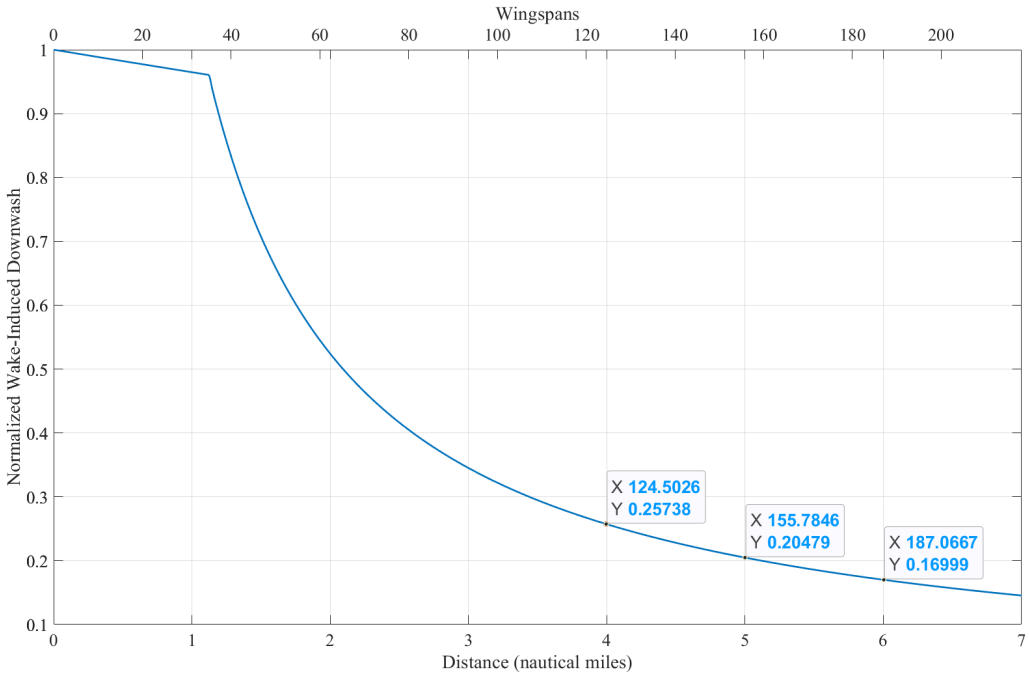

Figure 5: Wake decay from HEAVY Boeing 747-100 aircraft. The normalized downwash on the y-axis is the downwash at the input distance divided by the initial downwash when the distance is 0. The highlighted points indicate the number of wingspans downstream in X and the normalized downwash in Y.

being a LIGHT aircraft following a MEDIUM aircraft 5 nautical miles behind. Figure 6 plots the normalized downwash behind a UAM aircaft versus the downstream distance. The plot shows that at 5 nautical miles, the normalized downwash had reduced 0.0268, which is well below 0.205 normalized downwash at 5 nautical miles shown in Figure 5. Even at 4 nautical miles, the normalized downwash for the UAM aircraft was 0.0366 compared to 0.205 for the B747-100. It is clear that the existing separation criteria does not appropriately translate to UAM aircraft that are well below the LIGHT classification.

Instead of looking at existing separation criteria, we utilize the normalized downwash at the downwstream distances from Figure 5. Figure 6 also plots a line through 0.25 normalized downwash to indicate the largest allowable downwash as calculated by Figure 5. The UAM normalized downwash decayed to 0.25 at 130 wingspans, or 0.64 nautical miles. It is immediately apparent that the 0.25 normalized downwash threshold cannot directly translate to an urban UAM airspace because 0.64 nautical miles between aircraft is hardly a dense airspace, especially around vertiports with continuous taxiing. Therefore, it is necessary to evaluate the wake effect on the stability and dynamics of incoming aircraft to determine the threshold that should define the separation criteria. The dynamics testing will be completed in the final version of the manuscript.

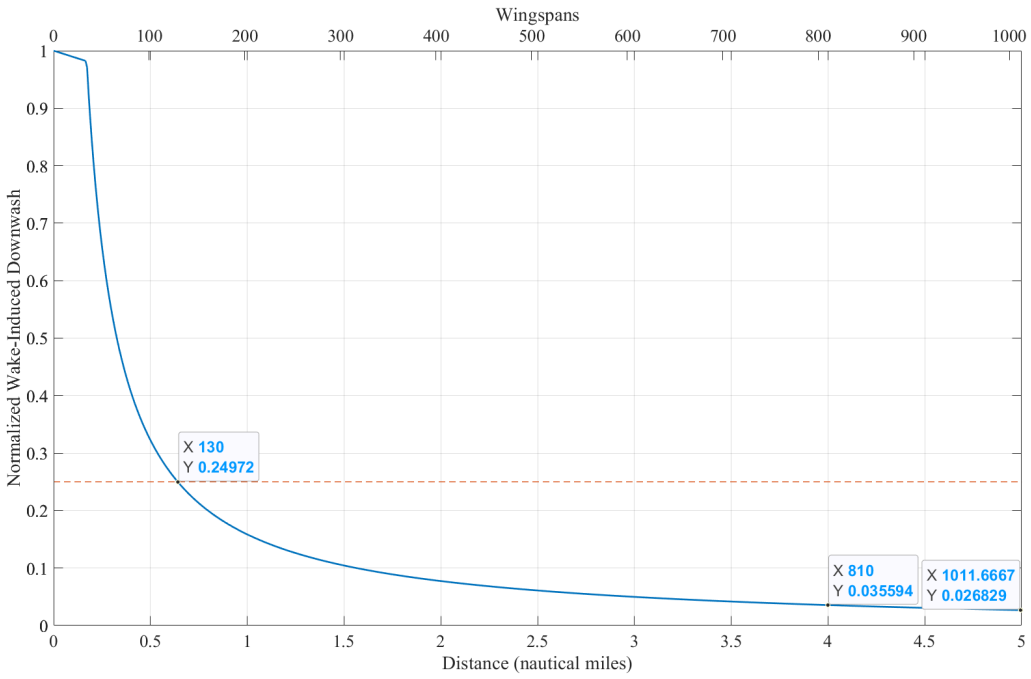

Figure 6: Wake decay from LIGHT UAM-type aircraft. The normalized downwash on the y-axis is the downwash at the input distance divided by the initial downwash when the distance is 0. The highlighted points indicate the number of wingspans downstream in X and the normalized downwash in Y.

B. Wake Area

We simulated four UAM-type fixed-wings traversing a 0.8 nm $\times$ 0.8 nm area to observe the wake-induced downwashes in semi-dense operations. Figure 7 shows the four UAM trajectories over the airspace. The aircraft were initialized and spaced so that the minimum separation was 0.8 nm. Figure 8 shows the downwash over the area in the z-direction with up being positive. To visualize the downwash values, we discretized the area to 10 ft $\times$ 10 ft cells and simulated one UAM's trajectory at a time. The induced downwash at a single cell was calculated over the simulation time window and then iterated throughout all cells in the wake area. After storing the wake velocity and aircraft trajectory information, this process was repeated for the other aircraft before finally summing up all of the wake velocities to get the cumulative downwash shown in Figure 8. Figure 9 highlights cells where the normalized downwash was above the 0.25 normalized downwash threshold.

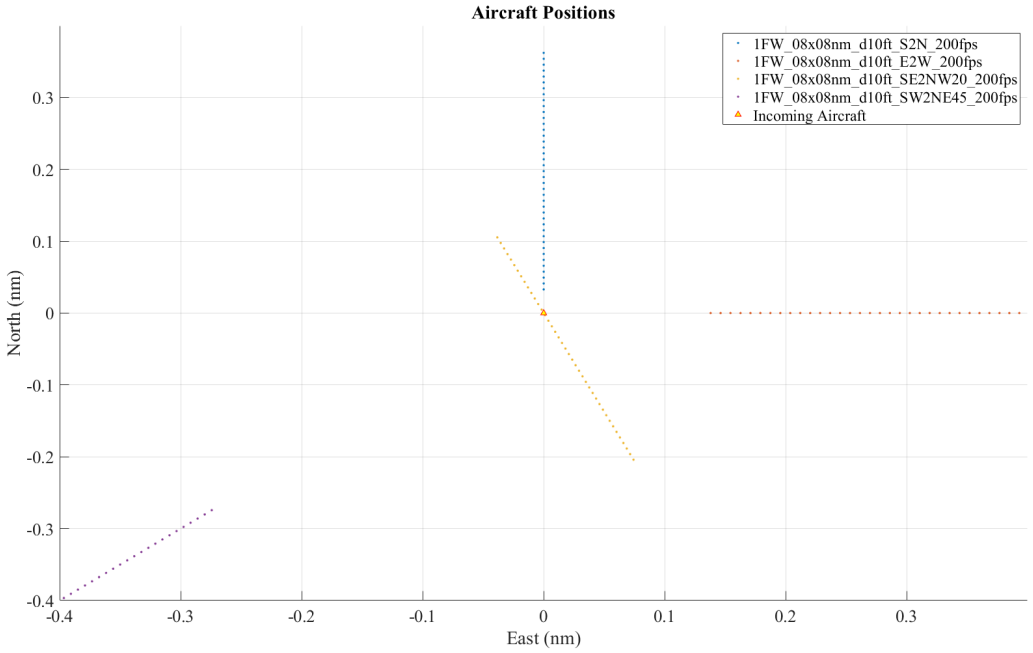

Figure 7: Four UAM aircraft trajectories.

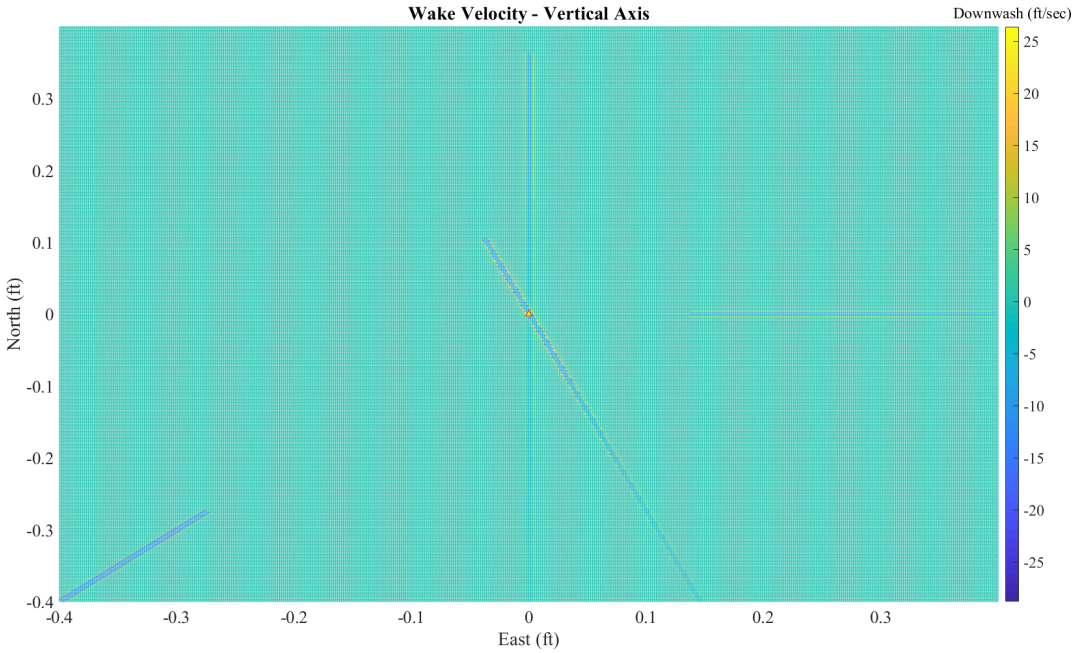

Figure 8: Four UAM aircraft wake-induced downwashes.

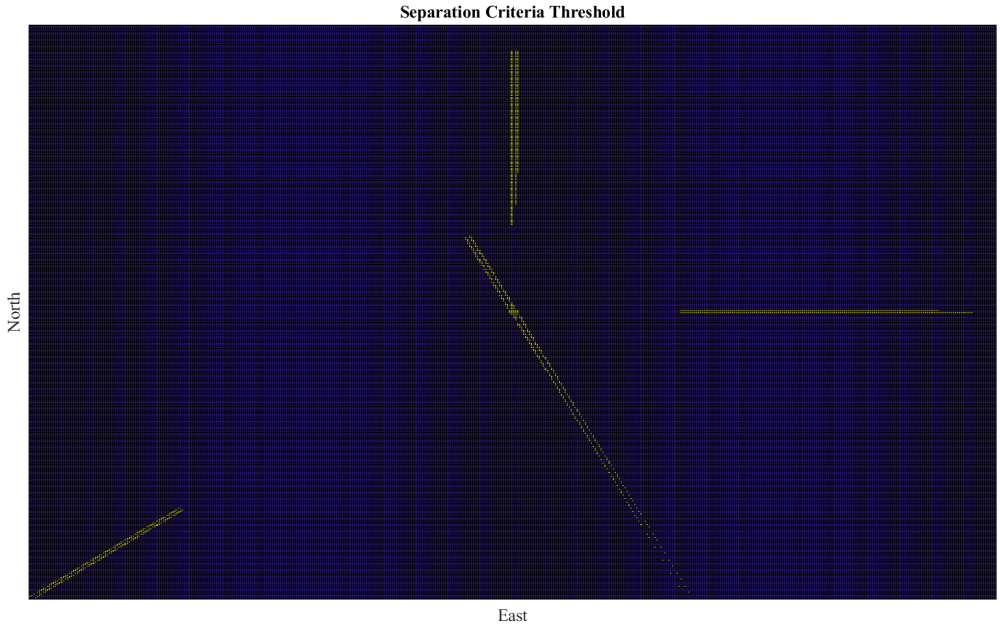

Figure 9: Four UAM aircraft downwash threshold. Cells highlighted in yellow indicate points where the downwash is greater than 0.25× the initial downwash at that particular cell.

Acknowledgments

This work was supported by the System-Wide Safety (SWS) project under the Airspace Operations and Safety Program within the NASA Aeronautics Research Mission Directorate (ARMD).

References

[1]Ellis, K., Koelling, J., Davies, M., and Krois, P., "In-time System-wide Safety Assurance (ISSA) Concept of Operations and Design Considerations for Urban Air Mobility (UAM)," *NASA/TM-2020-5003981*, 2020.

[2]Young, S., Ancel, E., Moore, A., Dill, E., Quach, C., Foster, J., Darafsheh, K., Smalling, K., Vazquez, S., Evans, E., et al., "Architecture and information requirements to assess and predict flight safety risks during highly autonomous urban flight operations," Tech. rep., 2020.

[3]Ahmad, N. N. and Proctor, F., "Review of idealized aircraft wake vortex models," *52nd Aerospace Sciences Meeting*, 2014, p. 0927.

[4]Sedin, Y.-J., Grasjoe, I., Kullberg, E., and Larsson, R., "A model for simulation of flight passages through trailing tip vortices," *ICAS 2002*, 2002.

[5]Tian, P., Chao, H., Gu, Y., and Hagerott, S. G., "UAV flight test evaluation of fusion algorithms for estimation of angle of attack and sideslip angle," *AIAA Guidance, Navigation, and Control Conference*, 2016, p. 0645.

[6]Nguyen, N. T., "A Physics-Based Spatial Wake Interactional Model of Fixed-Wing Aircraft and Rotorcraft for Urban Air Mobility," *AIAA Scitech 2021 Forum*, 2021, p. 0881.

[7]Nguyen, N. T., Bartolini, G., Baculi, J. E., Okolo, W., and Xiong, J., "Wake Vortex Interaction of Urban Air Mobility Aircraft," *AIAA SCITECH 2022 Forum*, 2022, p. 1031.

[8]Proctor, F., Hamilton, D., and Han, J., "Wake vortex transport and decay in ground effect-Vortex linking with the ground," *38th aerospace sciences meeting and exhibit*, 2000, p. 757.

[9]Proctor, F., Ahmad, N., Switzer, G., and Limon Duparcmeur, F., "Three-phased wake vortex decay," *AIAA Atmospheric and Space Environments Conference*, 2010, p. 7991.

[10]Burnham, D. C., Hallock, J. N., Tombach, I., Brashears, M., Barber, M., et al., "Ground-based measurements of the wake vortex characteristics of a B-747 aircraft in various configurations," Tech. rep., United States. Federal Aviation Administration, 1978.

[11](ICAO), I. C. A. O., "Doc. 4444.(ICAO), Procedures for Air Navigation Services Air Traffic Management," 2016.